Journal of Materials Chemistry B

ROYAL SOCIETY OF CHEMISTRY

PAPER

View Article Online
View Journal | View Issue

Cite this: J. Mater. Chem. B, 2020, 8, 6905

Phosphate-responsive 2D-metal–organic-framework-nanozymes for colorimetric detection of alkaline phosphatase†

Xiaoyu Wang, [a] Xiaoqian Jiang[a] and Hui Wei *[abc]

Received 11th November 2019,
Accepted 4th May 2020

DOI: 10.1039/c9tb02542a

rsc.li/materials-b

In this study, a simple colorimetric method with a tunable dynamic range for alkaline phosphatase (ALP) activity assay was developed by using a peroxidase-mimicking two-dimensional-metal–organic-framework (2D-MOF). Phosphates including pyrophosphate (PPi), ATP, and ADP inhibited the peroxidase-like activity of the 2D-MOF, while their hydrolytic product, phosphate (Pi), exhibited no such inhibitory ability. Therefore, by integrating with the ALP catalyzed hydrolytic reaction, a colorimetric method was developed for ALP activity quantification. Furthermore, by using different phosphates as inhibitors for the peroxidase-mimicking 2D-MOF, the dynamic range of this colorimetric method could be efficiently modulated. Three linear ranges of 2.5–20 U L^{-1}, 5–60 U L^{-1}, and 50–200 U L^{-1} could be obtained by using PPi, ATP, and ADP as inhibitors, respectively. Other proteins exhibited negligible interference, demonstrating that the proposed sensing method possessed excellent selectivity for ALP. Moreover, the developed assay was applied to evaluate ALP inhibitors and construct logic gates. This work not only provides a promising method for ALP detection but also represents a major step towards nanozyme bioanalysis.

Introduction

Alkaline phosphatase (ALP) plays pivotal roles in transphosphorylation and dephosphorylation of molecules containing phosphate esters in cells.[1,2] The abnormal expression of ALP is closely associated with many diseases, including bone disease, liver disease, and even prostate cancer.[3–6] In addition, the ALP levels may vary with age, gender and types of diseases.[6,7] For example, the serum ALP concentration in normal adults is 46–190 U L^{-1}, while it is higher (more than 500 U L^{-1}) in pregnant women and children.[8] Moreover, bone and liver-related diseases usually cause high activity of ALP, while hypophosphatasia and some other diseases may lead to a low concentration of ALP.[3,9] To date, various methods for ALP detection have been developed, including colorimetry, surface-enhanced Raman scattering (SERS), fluorescence spectroscopy, and electrochemical assays.[10–24] However, most of these methods only possessed a single dynamic range, which limited their applications for ALP detection under different physiological and pathological conditions. Therefore, the development of a cost-effective, label-free, and operation-simple method with a tunable dynamic range for quantitative detection of ALP is of great significance.

Nanozymes are considered to be promising enzyme mimics because they can not only overcome natural enzymes' intrinsic limitations but also possess unique properties in comparison with conventional artificial enzymes.[25–35] Recently, nanomaterials with peroxidase-like activities have exhibited broad applications for bioanalysis.[36–39] Many peroxidase-mimicking nanozymes were used to construct colorimetric sensors for the detection of various analytes including metal ions, biomolecules, cancer cells, *etc.*[36,37,40,41] Among these peroxidase-like nanozymes, the two-dimensional-metal–organic-framework (2D-MOF) exhibited unique advantages for bioanalysis due to not only its diverse and tailorable structures but also its highly exposed active sites for catalysis.[26,42–46] For example, Zhang and co-workers demonstrated that 2D metalloporphyrinic MOF nanosheets possessed excellent peroxidase-like activity.[44,45] Moreover, glucose oxidase-mimicking Au nanoparticles were grown on the surface of 2D-MOF nanosheets, enabling the cascade catalytic reactions for glucose detection.[44] Very recently, we demonstrated that sensor arrays constructed by three 2D-MOFs could be used for the detection and discrimination of phosphates as well as monitoring the phosphate-related enzymatic hydrolytic processes.[42]

[a] Department of Biomedical Engineering, College of Engineering and Applied Sciences, Nanjing National Laboratory of Microstructures, Jiangsu Key Laboratory of Artificial Functional Materials, Chemistry and Biomedicine Innovation Center (ChemBIC), Nanjing University, Nanjing, Jiangsu 210093, China. E-mail: weihui@nju.edu.cn; Web: http://weilab.nju.edu.cn; Fax: +86-25-83594648; Tel: +86-25-83593272

[b] State Key Laboratory of Analytical Chemistry for Life Science and State Key Laboratory of Coordination Chemistry, School of Chemistry and Chemical Engineering, Nanjing University, Nanjing, Jiangsu 210023, China

[c] Key Laboratory of Analytical Chemistry for Biology and Medicine (Wuhan University), Ministry of Education, Wuhan 430072, China

† Electronic supplementary information (ESI) available. See DOI: 10.1039/c9tb02542a

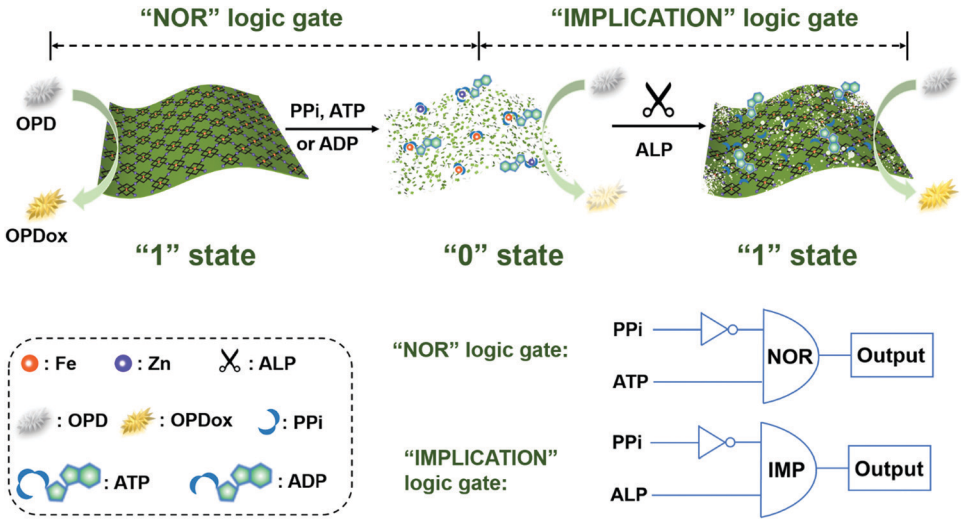

Scheme 1 Schematic illustration of the sensing platform constructed by the phosphate-responsive peroxidase-mimicking 2D-MOF for ALP activity assays and colorimetric logic gates.

In this study, colorimetric assays with a tunable dynamic range were developed for monitoring the ALP activity by using peroxidase-mimicking 2D Zn-TCPP(Fe) nanozymes (Scheme 1). A 2D-MOF with excellent peroxidase-like activity was first synthesized and characterized. Furthermore, we have recently demonstrated that PPi, ATP, and ADP could effectively inhibit the catalytic activity of 2D-MOF-nanozymes, while their hydrolytic product (*i.e.*, Pi) exhibited negligible effect.[42] On the basis of this principle, by coupling with the ALP-catalyzed hydrolytic reaction, the ALP activity assay could be constructed. Moreover, the dynamic range of the colorimetric method for ALP could be efficiently modulated when different phosphates (*i.e.*, PPi, ATP, and ADP) were applied to inhibit the peroxidase-like activity of the 2D-MOF. In addition, colorimetric logic gates could be rationally constructed on the basis of the ALP sensing platform (Scheme 1). Overall, this study demonstrated a colorimetric method with a tunable dynamic range for sensitive and selective detection of ALP activity.

Experimental section

Chemicals and materials

All reagents were at least of analytical grade. Adenosine 5′-triphosphate disodium salt (ATP), adenosine 5′-diphosphate sodium salt (ADP), 3,3′,5,5′-tetramethylbenzidine dihydrochloride (TMB), 2,2′-azinobis(3-ethyl benzothi-azoline-6-sulfonic acid)ammonium (ABTS), zinc nitrate hexahydrate ($Zn(NO_3)\cdot 6H_2O$), bovine serum albumin (BSA), trypsin, glucose oxidase (GOx), α-amylase, and hydrogen peroxide were purchased from Aladdin Chemical Reagent Co., Ltd. Human serum albumin (HSA) was purchased from CSL Behring AG (Switzerland). *N*,*N*-Dimethylformamide (DMF), *o*-phenylenediamine (OPD), and sodium acetate trihydrate were purchased from Sinopharm Chemical Reagent Co., Ltd. Polyvinylpyrrolidone (PVP, MW 40 000), lysozyme, and alkaline phosphatase were purchased from Sigma-Aldrich. Sodium pyrophosphate (PPi) and sodium orthovanadate (Na_3VO_4) were purchased from Kermel Reagent. Fe(III) tetra(4-carboxyphenyl)porphine chloride (TCPP(Fe)) was purchased from J&K Scientific Co. Ltd. All aqueous solutions used in the experiments were prepared with deionized water (18.2 MΩ cm, Millipore).

Instrumentation

TEM images were recorded on a JEOL JEM-2100 transmission electron microscope at an acceleration voltage of 200 kV. UV-visible absorption spectra were collected using a spectrophotometer (TU-1900, Beijing Purkinje General Instrument Co. Ltd, China). The absorption of a 96-well plate at 450 nm was recorded by using a SpectraMax M2e microplate reader (Molecular Devices, USA).

Synthesis of 2D Zn-TCPP(Fe). The 2D Zn-TCPP(Fe) was synthesized according to our previous method.[42,43] Briefly, 3.0 mg of $Zn(NO_3)_2\cdot 6H_2O$, 0.8 mg of pyrazine, and 20.0 mg of PVP (MW 40 000) were dissolved in 12 mL of ethanol–DMF mixture (v : v = 1 : 3). Subsequently, 4.4 mg TCPP(Fe) dissolved in 4 mL of ethanol–DMF mixture (v : v = 1 : 3) was added dropwise into the above solution under vigorous stirring. The mixture solution was then heated up to 80 °C and kept for 24 h.

Effects of PPi, ATP, and ADP on the peroxidase-like activity of Zn-TCPP(Fe). 2.5 μL of 2D Zn-TCPP(Fe) with a concentration of 100 μg mL^{-1}, 2.5 μL of various concentrations of PPi (ATP or ADP), and 75 μL of NaOAc (0.2 M, pH 4.5) were incubated for 20 min in a 96-well plate. After that, 10 μL of H_2O_2 (1 M) and 10 μL of OPD (20 mM) were added into the above solution. The absorption of each well was consecutively recorded every 2.5 min for 20 min by using a microplate reader.

Colorimetric ALP activity assay. A colorimetric ALP activity assay was performed as follows. 4 μL of 500 μM of PPi (ATP or ADP), 20 μL of ALP with various concentrations, and 76 μL of Tris–HCl (50 mM, pH 7.4) were first incubated for 30 min at 37 °C. Then, 10 μL of the above incubated solution, 2.5 μL of 2D-MOF (100 μg mL^{-1}), and 67.5 μL of NaOAc buffer (0.2 M, pH 4.5)

were added into each well of a 96-well plate. The mixture was further incubated for 20 min. Subsequently, 10 μL of H_2O_2 (1 M) and 10 μL of OPD (20 mM) were added into the above solution, respectively. Immediately after the addition of OPD, the absorption of each well was consecutively recorded every 2.5 min for 20 min by using a microplate reader.

Inhibitory effect of Na_3VO_4 on ALP. To demonstrate the potential application of the developed colorimetric assay for ALP inhibitor investigation, 5 μL of Na_3VO_4 aqueous solution with various concentrations, 50 μL of ALP aqueous solution (2000 U L^{-1}), and 45 μL of Tris–HCl buffer (50 mM, pH 7.4) were incubated at 37 °C for 30 min. Subsequently, the experimental procedures were the same as the ALP activity assay.

Results and discussion

Colorimetric detection of ALP

A 2D-MOF with a typical sheet-like structure was synthesized by a surfactant-assisted method (Fig. S1, ESI†). The peroxidase-like activity of the 2D-MOF was first investigated by monitoring the catalytic oxidation of OPD in the presence of H_2O_2. The oxidized product of OPD (*i.e.*, OPDox) possessed a characteristic absorption peak at 450 nm. As shown in Fig. S2a (ESI†), the reaction system exhibited a strong absorption value at 450 nm in the presence of H_2O_2, OPD, and 2D-MOF nanozymes. Other control groups containing OPD, H_2O_2 and OPD, or 2D-MOF and OPD, possessed negligible absorption. In addition to OPD, other typical peroxidase substrates, such as TMB and ABTS could also be catalytically oxidized by the 2D-MOF in the presence of H_2O_2 (Fig. S2b, ESI†). Moreover, the peroxidase-like activity of the 2D-MOF strongly depended on the catalyst concentration and H_2O_2 concentration (Fig. S2c and d, ESI†). The excellent catalytic activity of the 2D-MOF was attributed to the active sites of TCPP(Fe), while the Zn^{2+} ions served as the junction sites.

Having demonstrated the excellent peroxidase-like activity of the 2D-MOF, we further attempted to modulate its catalytic activity by phosphates. As shown in Fig. 1a, the activity of the 2D-MOF could be significantly inhibited by PPi, while Pi showed negligible effect on the peroxidase-like activity of the

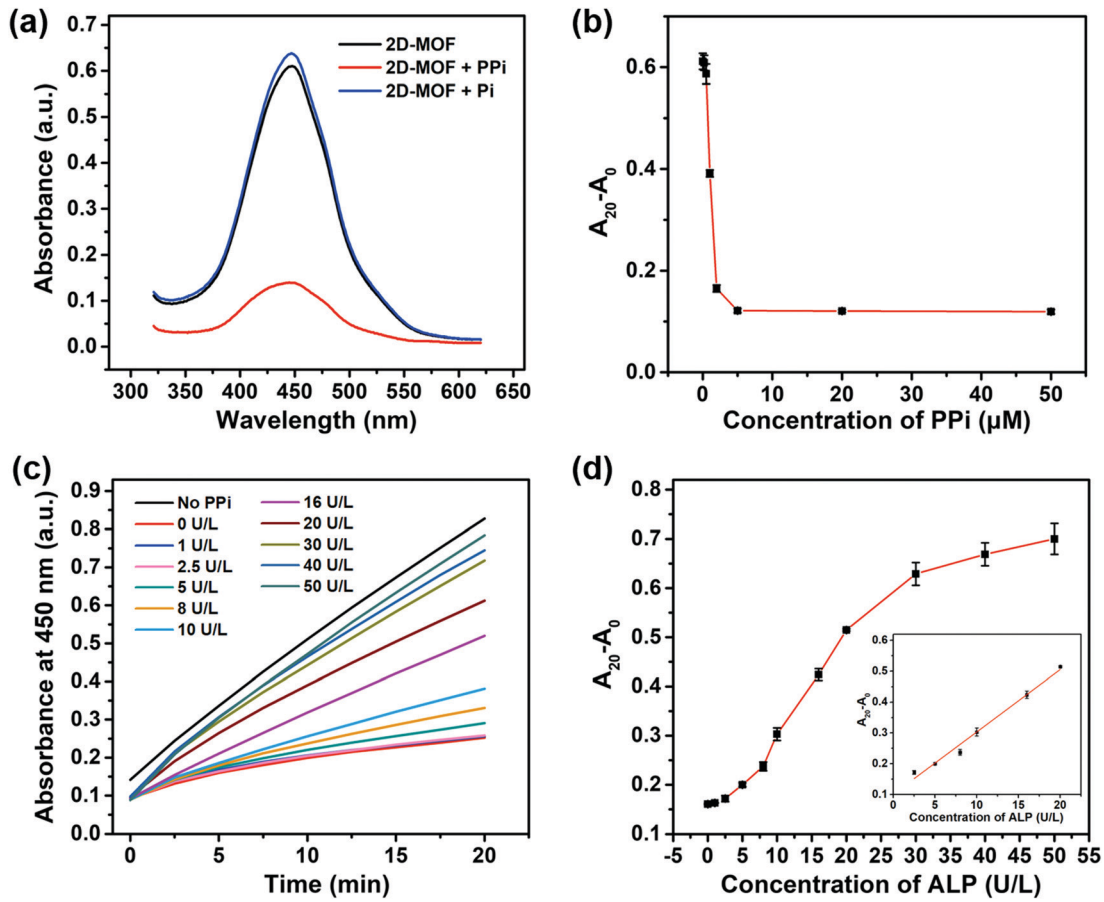

Fig. 1 (a) Typical absorption spectra for monitoring the catalytic oxidation of 2 mM of OPD in various reaction systems of (I) 2.5 μg mL^{-1} of 2D-MOF, (II) 2.5 μg mL^{-1} of 2D-MOF + 2 μM of PPi, and (III) 2.5 μg mL^{-1} of 2D-MOF + 2 μM of Pi. (b) The relative change of absorption of OPDox ($A_{20} - A_0$) in the presence of various concentrations of PPi. (c) Kinetic curves of the absorption of 450 nm for different concentrations of ALP in the presence of 2.5 μg mL^{-1} of 2D-MOF and 2 μM of PPi. (d) The relative change of absorption of OPDox ($A_{20} - A_0$) *versus* the concentration of ALP. Inset: Linear calibration plot of the relative change of absorption against ALP activity. A_{20} and A_0 were the absorption of OPDox at 450 nm at 0 min and 20 min. Each error bar shows the standard deviation of three independent measurements.

2D-MOF. As shown in Fig. 1b and Fig. S3 (ESI†), the absorption of OPDox at 450 nm decreased with the increase of the PPi concentration, demonstrating that the inhibitory effect depended on the PPi concentration. The inhibitory mechanism was demonstrated in our previous study.[42] Phosphates can first chelate with Zn^{2+} to trigger the structure collapse of the 2D-MOF. Subsequently, the phosphates can further bind with the catalytically active sites (*i.e.*, Fe) in TCPP(Fe), which in turn resulted in the decrease of their catalytic activity. The mechanism was demonstrated by transmission electron microscopy (TEM) imaging. As shown in Fig. S4a and b (ESI†), the sheet-like structure of the 2D-MOF was destroyed when PPi was added into the solution.

Because PPi and Pi exhibited differential effects on the catalytic activity of the 2D-MOF, and ALP could catalyze the hydrolysis of PPi to Pi, a colorimetric method could be constructed for ALP by phosphate-mediated peroxidase-like activity. The dependence of the peroxidase-like activity of the 2D-MOF on the ALP concentration was further studied (Fig. 1c). As shown in Fig. 1d, the relative change of absorption of OPDox ($A_{20} - A_0$) increased with the increase of the ALP concentration ranging from 1 to 50 U L^{-1} because ALP catalyzed the hydrolysis of PPi to prevent its inhibitory effect on the 2D-MOF. A linear dependence between $A_{20} - A_0$ and ALP concentrations in the range of 2.5 to 20 U L^{-1} could be obtained. TEM images also demonstrated that the sheet-like structure of the 2D-MOF was intact in the presence of ALP, which was consistent with the maintained high peroxidase-like activity (Fig. S4c and d, ESI†).

Tunable dynamic range

It is of great importance to develop ALP activity assays with a tunable dynamic range because the concentration of ALP may vary with age, gender, and types of diseases.[6,7] In addition to PPi, ATP and ADP also inhibited the peroxidase-like activity of the 2D-MOF (Fig. S5a and S6a, ESI†). Compared with PPi, the inhibitory abilities of ATP and ADP were weaker (Fig. 1b and 2a, c). We envisioned that the dynamic range of the colorimetric method for ALP activity may be modulated by replacing PPi with ATP or ADP in the assay. As shown in Fig. 2a and c, 5 μM of ATP and 30 μM of ADP were selected for ALP activity assay, respectively. For ATP-mediated ALP detection, the dynamic range of this colorimetric method could be tuned to 5–60 U L^{-1} (Fig. S5b (ESI†) and Fig. 2b). The dynamic range could be further modulated to 50–200 U L^{-1} by ADP-mediated ALP detection (Fig. S6b (ESI†) and Fig. 2d). Therefore, the quantification of ALP activity over different concentration ranges could be achieved by using the developed sensing systems.

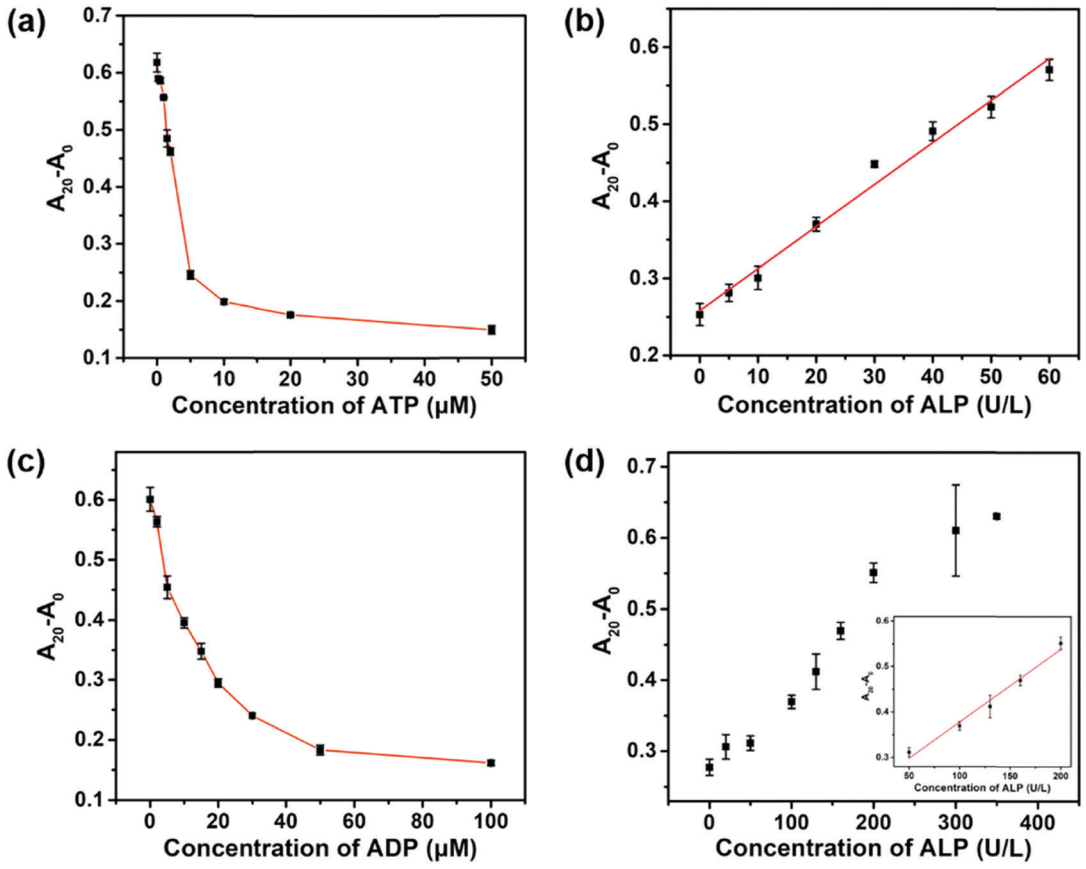

Fig. 2 The relative change of absorption of OPDox ($A_{20} - A_0$) in the presence of various concentrations of (a) ATP and (c) ADP. The relative change of absorption of OPDox ($A_{20} - A_0$) *versus* the concentration of ALP based on (b) 5 μM of ATP and 2.5 μg mL^{-1} of 2D-MOF systems, and (d) 30 μM of ADP and 2.5 μg mL^{-1} of 2D-MOF systems. Inset: Linear calibration plot of the relative change of absorption against ALP activity based on ADP and 2D-MOF systems. Each error bar shows the standard deviation of three independent measurements.

Selectivity

To demonstrate the selectivity of the proposed method, the effect of several potential interfering proteins such as lysozyme (Lys), bovine serum albumin (BSA), trypsin (Try), human serum albumin (HSA), amylase (Amy), and glucose oxidase (GOx) was investigated. The concentrations of ALP and other proteins used in this selectivity assay were 20 U L^{-1} and 20 nM, respectively. As shown in Fig. 3 and Fig. S7 (ESI†), only ALP remarkedly increased the peroxidase-like activity of the 2D-MOF, while other proteins exhibited a similar absorption value at 450 nm with blank, implying the good specificity of this colorimetric method for sensing of ALP. The excellent selectivity of this assay should be attributed to the specific hydrolysis of PPi by ALP enzymes.

Inhibition assay

Screening the enzyme inhibitors is greatly important in drug design.[47] Having demonstrated the ability of the as-designed colorimetric method for ALP detection, we further investigated whether this method could be applied for evaluating the enzyme inhibitor efficiency. Previous studies reported that sodium orthovanadate (Na_3VO_4) is a reversible and competitive inhibitor for ALP.[14] Therefore, Na_3VO_4 was taken as an example for proof-of-concept experiments. To validate the inhibition assay, ALP was first preincubated with Na_3VO_4 with various concentrations in aqueous solutions for 30 min. Then, Na_3VO_4-treated ALP solutions were mixed with PPi for another 30 min. Furthermore, 2D-MOF nanozymes were added into the above incubated solutions and subsequently subjected to peroxidase-like activities measurements. If the ALP could be efficiently inhibited by Na_3VO_4, the hydrolysis of PPi by ALP would be restricted, and as a consequence, the catalytic activity of the 2D-MOF would be decreased. As shown in Fig. 4a and Fig. S8 (ESI†), the absorption of OPDox catalyzed by the 2D-MOF decreased with the increasing concentrations of Na_3VO_4, demonstrating that the Na_3VO_4 remarkably inhibited the activity of ALP. To quantify the inhibiting ability, the inhibition ratio (I, %) was defined by the following regression equation: $I\ (\%) = \frac{A_1 - A_2}{A_1 - A_0} \times 100$, where A_0 was the relative change of the absorption at 450 nm in the absence of ALP, A_1 was the relative change of the absorption at 450 nm in the

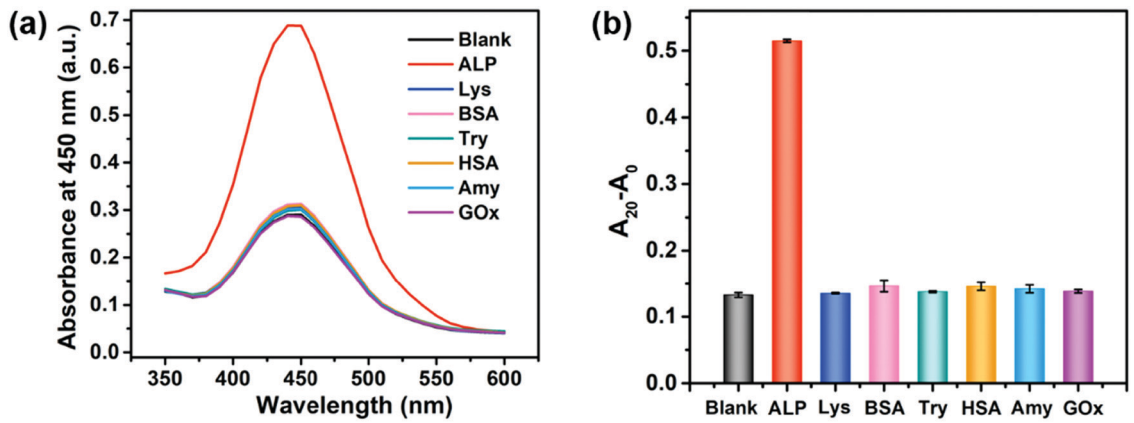

Fig. 3 (a) Typical absorption spectra and (b) the relative change of the absorption of OPDox catalyzed by 2.5 μg mL^{-1} of the 2D-MOF with 2 μM of PPi in the absence and presence of 20 U L^{-1} of ALP, and 20 nM of Lys, BSA, Try, HSA, Amylase, and GOx. A_{20} and A_0 were the absorption of OPDox at 450 nm at 0 min and 20 min, respectively. Each error bar shows the standard deviation of three independent measurements.

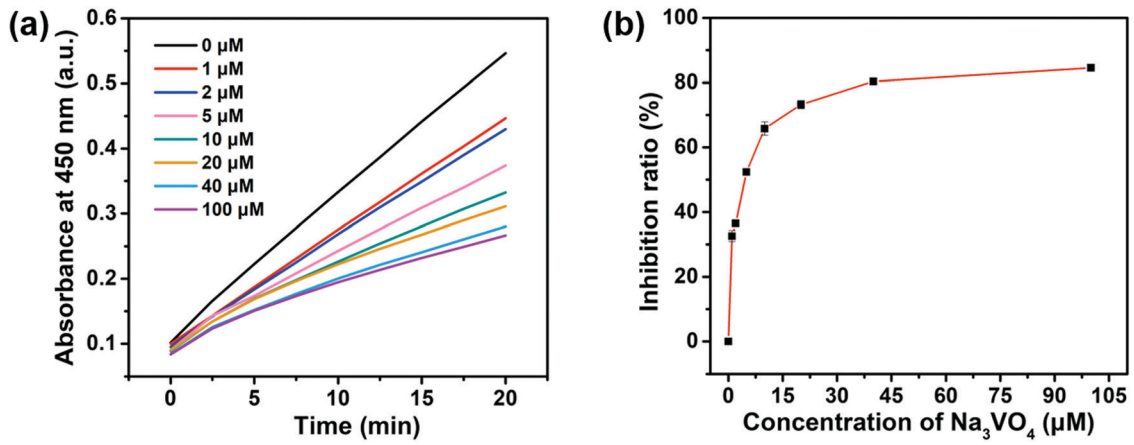

Fig. 4 (a) Kinetics curves of the absorption of ALP responsive reaction systems in the presence of various concentrations of Na_3VO_4. (b) The dependence of the inhibition ratio on the concentration of Na_3VO_4. Each error bar shows the standard deviation of three independent measurements.

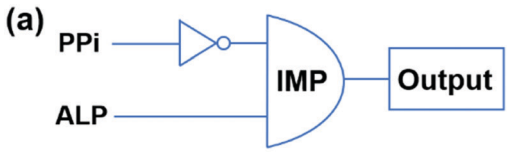

Input 1	Input 2	Output
PPi	ALP	Absorbance
0	0	1
1	0	0
0	1	1
1	1	1

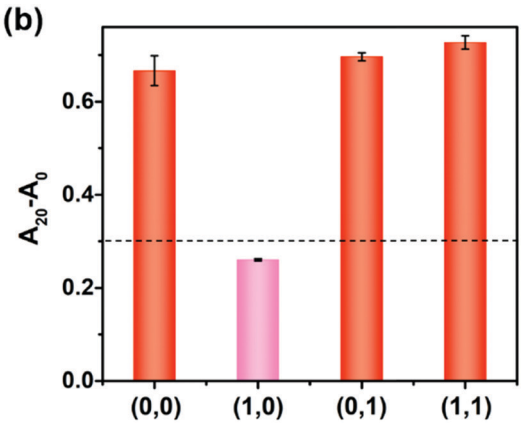

Fig. 5 The "IMPLICATION" logic gate by using PPi and ALP as inputs and the absorption at 450 nm as output. (a) Schematic as well as the truth table and (b) the histogram of the "IMPLICATION" logic gate. Each error bar shows the standard deviation of three independent measurements.

presence of ALP without the inhibitor, and A_2 was the relative change of the absorption at 450 nm in the presence of ALP and inhibitor. The dependence of the inhibition ratio on the concentration of Na_3VO_4 is plotted in Fig. 4b. These results demonstrated that the current colorimetric assay for ALP could also be applied for evaluating the ALP inhibitor efficiency.

Logic gates

Molecular logic gates have found interesting applications in biosensing and medical diagnostics.[17,48] Herein, on the basis of the peroxidase-like activity of the 2D-MOF modulated by PPi and ALP, an "IMPLICATION" logic gate was constructed (Fig. 5). In this logic gate, PPi and ALP were used as inputs, and the absorption values of OPDox at 450 nm acted as the output signals (Fig. 5a). For input, "0" and "1" states were defined in the absence and presence of PPi and ALP, respectively. For output, the absorption value of more than 0.3 was regarded as "1", while less than 0.3 was defined as "0". As shown in Fig. 5b, when the PPi alone was applied (0,1), the catalytic activity of the 2D-MOF could be efficiently inhibited and the output was "0". In other cases, the 2D-MOF exhibited excellent peroxidase-like activities and the output was "1". In addition to an "IMPLICATION" logic gate, an "INHIBIT" could be developed by using PPi and 2D-MOF as inputs, and a "NOR" logic gate could be constructed by using PPi and ATP as inputs, respectively (Fig. S9 and S10, ESI†). These above results demonstrated the potential applications of the colorimetric assay for construction of logic gates.

Conclusions

In conclusion, a colorimetric ALP activity assay with high selectivity was developed by using phosphate-responsive 2D-MOF nanozymes. Moreover, the dynamic range was rationally tuned when different phosphates (PPi, ATP, or ADP) were applied for inhibiting the peroxidase-like activity of the 2D-MOF. In addition to ALP detection, this colorimetric method exhibited broad applications for evaluating the ALP enzyme inhibitor (*i.e.*, Na_3VO_4) and constructing logic gates. Overall, this method with the advantages of simplicity, excellent selectivity, and tunable dynamic range exhibited potential applications for biomedical diagnosis.

Conflicts of interest

There are no conflicts to declare.

Acknowledgements

This work was supported by the China Postdoctoral Science Foundation (2019TQ0144 and 2019M661786), the National Natural Science Foundation of China (21722503, 21874067, and 91859112), the 973 Program (2015CB659400), the PAPD Program, the Shuangchuang Program of Jiangsu Province, Open Funds of the State Key Laboratory of Analytical Chemistry for Life Science (SKLACLS1704), Open Funds of the State Key Laboratory of Coordination Chemistry (SKLCC1819), Open Funds of Key Laboratory of Analytical Chemistry for Biology and Medicine (Wuhan University), Ministry of Education (ACBM2019001) and Fundamental Research Funds for the Central Universities (021314380145).

References

1 J.-P. Lalles, *Nutr. Rev.*, 2014, **72**, 82–94.
2 H. Wei, C. Chen, B. Han and E. Wang, *Anal. Chem.*, 2008, **80**, 7051–7055.
3 K. Kaliannan, S. R. Hamarneh, K. P. Economopoulos, S. N. Alam, O. Moaven, P. Patel, N. S. Malo, M. Ray, S. M. Abtahi, N. Muhammad, A. Raychowdhury, A. Teshager, M. M. R. Mohamed, A. K. Moss, R. Ahmed, S. Hakimian, S. Narisawa, J. L. Millan, E. Hohmann, H. S. Warren, A. K. Bhan, M. S. Malo and R. A. Hodin, *Proc. Natl. Acad. Sci. U. S. A.*, 2013, **110**, 7003–7008.
4 P. Garnero and P. D. Delmas, *J. Clin. Endocrinol. Metab.*, 1993, **77**, 1046–1053.
5 L. F. A. Wymenga, J. H. B. Boomsma, K. Groenier, D. A. Piers and H. J. A. Mensink, *BJU Int.*, 2001, **88**, 226–230.

6 J. Lee, C. T. Bubar, H. G. Moon, J. Kim, A. Busnaina, H. Lee and S. J. Shefelbine, *ACS Sens.*, 2018, **3**, 2709–2715.
7 J. R. Eastman and D. Bixler, *Clin. Chem.*, 1977, **23**, 1769–1770.
8 T. U. Hausamen, R. Helger, W. Rick and W. Gross, *Clin. Chim. Acta*, 1967, **15**, 241–245.
9 M. P. Whyte, C. R. Greenberg, N. J. Salman, M. B. Bober, W. H. McAlister, D. Wenkert, B. J. Van Sickle, J. H. Simmons, T. S. Edgar, M. L. Bauer, M. A. Hamdan, N. Bishop, R. E. Lutz, M. McGinn, S. Craig, J. N. Moore, J. W. Taylor, R. H. Cleveland, W. R. Cranley, R. Lim, T. D. Thacher, J. E. Mayhew, M. Downs, J. L. Millan, A. M. Skrinar, P. Crine and H. Landy, *N. Engl. J. Med.*, 2012, **366**, 904–913.
10 S. Goggins, C. Naz, B. J. Marsh and C. G. Frost, *Chem. Commun.*, 2015, **51**, 561–564.
11 L. Dong, Q. Miao, Z. Hai, Y. Yuan and G. Liang, *Anal. Chem.*, 2015, **87**, 6475–6478.
12 J. Deng, P. Yu, Y. Wang and L. Mao, *Anal. Chem.*, 2015, **87**, 3080–3086.
13 Z. Guo, X. Zhu, S. Wang, C. Lei, Y. Huang, Z. Nie and S. Yao, *Nanoscale*, 2018, **10**, 19579–19585.
14 J. Li, L. Si, J. Bao, Z. Wang and Z. Dai, *Anal. Chem.*, 2017, **89**, 3681–3686.
15 G. Li, H. Fu, X. Chen, P. Gong, G. Chen, L. Xia, H. Wang, J. You and Y. Wu, *Anal. Chem.*, 2016, **88**, 2720–2726.
16 C. Ruan, W. Wang and B. Gu, *Anal. Chem.*, 2006, **78**, 3379–3384.
17 Y. Han, Y. Niu, M. Liu, F. Niu and Y. Xu, *J. Mater. Chem. B*, 2019, **7**, 897–902.
18 K. Ye, L. Wang, H. Song, X. Li and X. Niu, *J. Mater. Chem. B*, 2019, **7**, 4794–4800.
19 H. Song, K. Ye, Y. Peng, L. Wang and X. Niu, *J. Mater. Chem. B*, 2019, **7**, 5834–5841.
20 P. Ni, J. Xie, C. Chen, Y. Jiang, Z. Zhao, Y. Zhang, Y. Lu and J. Yu, *Microchim. Acta*, 2019, **186**, 320.
21 C. M. Li, S. J. Zhen, J. Wang, Y. F. Li and C. Z. Huang, *Biosens. Bioelectron.*, 2013, **43**, 366–371.
22 P. Zhang, C. Fu, Q. Zhang, S. Li and C. Ding, *Anal. Chem.*, 2019, **91**, 12377–12383.
23 Q. Zhang, S. Li, C. Fu, Y. Xiao, P. Zhang and C. Ding, *J. Mater. Chem. B*, 2019, **7**, 443–450.
24 Q. Chen, S. Li, Y. Liu, X. Zhang, Y. Tang, H. Chai and Y. Huang, *Sens. Actuators, B*, 2020, **305**, 127511.
25 H. Wei and E. Wang, *Chem. Soc. Rev.*, 2013, **42**, 6060–6093.
26 J. Wu, X. Wang, Q. Wang, Z. Lou, S. Li, Y. Zhu, L. Qin and H. Wei, *Chem. Soc. Rev.*, 2019, **48**, 1004–1076.
27 Y. Huang, J. Ren and X. Qu, *Chem. Rev.*, 2019, **119**, 4357–4412.
28 L. Gao, J. Zhuang, L. Nie, J. Zhang, Y. Zhang, N. Gu, T. Wang, J. Feng, D. Yang, S. Perrett and X. Yan, *Nat. Nanotechnol.*, 2007, **2**, 577–583.
29 X. Wang, X. J. Gao, L. Qin, C. Wang, L. Song, Y.-N. Zhou, G. Zhu, W. Cao, S. Lin, L. Zhou, K. Wang, H. Zhang, Z. Jin, P. Wang, X. Gao and H. Wei, *Nat. Commun.*, 2019, **10**, 704.
30 D. Jiang, D. Ni, Z. T. Rosenkrans, P. Huang, X. Yan and W. Cai, *Chem. Soc. Rev.*, 2019, **48**, 3683–3704.
31 H. Dong, Y. Fan, W. Zhang, N. Gu and Y. Zhang, *Bioconjugate Chem.*, 2019, **30**, 1273–1296.
32 W. Zhang, S. Hu, J.-J. Yin, W. He, W. Lu, M. Ma, N. Gu and Y. Zhang, *J. Am. Chem. Soc.*, 2016, **138**, 5860–5865.
33 B. Liu and J. Liu, *Nano Res.*, 2017, **10**, 1125–1148.
34 L. Huang, J. Chen, L. Gan, J. Wang and S. Dong, *Sci. Adv.*, 2019, **5**, eaav5490.
35 S. Li, L. Wang, X. Zhang, H. Chai and Y. Huang, *Sens. Actuators, B*, 2018, **264**, 312–319.
36 W. Song, B. Zhao, C. Wang, Y. Ozaki and X. Lu, *J. Mater. Chem. B*, 2019, **7**, 850–875.
37 X. Wang, Y. Hu and H. Wei, *Inorg. Chem. Front.*, 2016, **3**, 41–60.
38 Z. Gao, H. Ye, D. Tang, J. Tao, S. Habibi, A. Minerick, D. Tang and X. Xia, *Nano Lett.*, 2017, **17**, 5572–5579.
39 S. Li, X. Hu, Q. Chen, X. Zhang, H. Chai and Y. Huang, *Biosens. Bioelectron.*, 2019, **137**, 133–139.
40 X. Wang, L. Qin, M. Zhou, Z. Lou and H. Wei, *Anal. Chem.*, 2018, **90**, 11696–11702.
41 X. Wang, L. Qin, M. Lin, H. Xing and H. Wei, *Anal. Chem.*, 2019, **91**, 10648–10656.
42 L. Qin, X. Wang, Y. Liu and H. Wei, *Anal. Chem.*, 2018, **90**, 9983–9989.
43 H. Cheng, Y. Liu, Y. Hu, Y. Ding, S. Lin, W. Cao, Q. Wang, J. Wu, F. Muhammad, X. Zhao, D. Zhao, Z. Li, H. Xing and H. Wei, *Anal. Chem.*, 2017, **89**, 11552–11559.
44 Y. Huang, M. Zhao, S. Han, Z. Lai, J. Yang, C. Tan, Q. Ma, Q. Lu, J. Chen, X. Zhang, Z. Zhang, B. Li, B. Chen, Y. Zong and H. Zhang, *Adv. Mater.*, 2017, **29**, 1700102.
45 Y. Wang, M. Zhao, J. Ping, B. Chen, X. Cao, Y. Huang, C. Tan, Q. Ma, S. Wu, Y. Yu, Q. Lu, J. Chen, W. Zhao, Y. Ying and H. Zhang, *Adv. Mater.*, 2016, **28**, 4149–4155.
46 S. Li, X. Liu, H. Chai and Y. Huang, *TrAC, Trends Anal. Chem.*, 2018, **105**, 391–403.
47 X. Li, Z. Zheng, X. Liu, S. Zhao and S. Liu, *Biosens. Bioelectron.*, 2015, **64**, 1–5.
48 X. Ji, H. Lv, M. Ma, B. Lv and C. Ding, *Microchim. Acta*, 2017, **184**, 2505–2513.